Available online at www.sciencedirect.com
SCIENCE DIRECT®
Physica B 336 (2003) 56–62
PHYSICA B
www.elsevier.com/locate/physb

Sources of decoherence in beamline optics

I.K. Robinson*, C.A. Kenney-Benson, I.A. Vartanyants

Department of Physics and Materials Research Laboratory, University of Illinois, Urbana, USA

Received 7 November 2002; accepted 5 February 2003

Abstract

Coherent X-ray diffraction (CXD) is a potentially important technique for the study of surfaces and interfaces. The level of coherence achievable in a given situation is a function of both the instrumentation used and the source of X-rays. Coherence can be lost by certain kinds of imperfection within these components. Here, we present some elementary principles for the preservation of coherence in a typical synchrotron radiation beamline. These will be illustrated with results from the Sector 34 CXD beamline at the advanced photon source. The consequences for diffraction imaging of surfaces and interfaces with CXD are also discussed in this paper.

Keywords: Coherence; X-ray diffraction; Decoherence; Surfaces

Coherent X-ray diffraction (CXD) is one of the techniques that has become routinely available since the construction of third-generation sources of synchrotron radiation (SR) in the X-ray wavelength range [1]. Because CXD is a brightness-limited application with relatively weak signal levels, it has fully benefited from the three orders-of-magnitude improvements of source brightness. In recent years, two versions of CXD experiments have become popular: X-ray photon correlation spectroscopy for studying fluctuations on atomic length scales and the application to imaging structure with resolution in the nanometer range. In this paper we focus more on the second application and how it can be optimized by appropriate design of the beamline instrumentation. However, the results should be equally applicable to all methods that depend on preservation of coherence.

Coherence is usually divided into its longitudinal and transverse components [2]. Here, we will not discuss further the longitudinal part, which relates to the monochromaticity or wavelength-spread, $\Delta\lambda/\lambda$, of the beam, except to say that it couples to the sample geometry via the optical path-length difference (OPLD); a sufficiently good monochromator must be used that the maximum OPLD is kept smaller than the longitudinal coherence length, $L_L = \frac{1}{2}\lambda^2/\Delta\lambda$ [3]. This experimental challenge is a different subject that is largely uncoupled from that of the transverse coherence, which is our present topic. We will instead make the assumption here that the radiation is perfectly monochromatic. Needless to say, the loss of *either* longitudinal or transverse coherence will cause the necessary measurements of a CXD experiment to become smeared in such a

*Corresponding author: MRL 172, Department of Physics, University of Illinois at Urbana-Champaign 1110 West Green Street, Urbana, IL 61801-3080, USA.
E-mail address: ikr@uiuc.edu (I.K. Robinson).

0921-4526/03/$ - see front matter
doi:10.1016/S0921-4526(03)00269-2

way as to reduce their usefulness or else to introduce undesirable artifacts.

Transverse coherence is usually considered to be a consequence of the finite size of the spatial distribution of the source. The big technological advances in SR sources have improved this characteristic considerably, with present-day source sizes of 600 μm horizontally and 40 μm vertically [4]. If each point in the source is considered to be the origin of a spherical wave, then two points, d apart, lead to waves that do not superimpose perfectly; if these waves are in phase at one place on the sample than they will be out of phase a lateral distance $\lambda D/2d$ away. The source-to-sample distance is D here. This defines the lateral coherence length L_T of a distributed source of width 2σ as [3],

$$L_T = \frac{\lambda D}{4\sigma}. \quad (1)$$

Direct substitution in this formula for a typical beamline with $D = 50$ m gives lateral coherence lengths of several microns. This has motivated CXD experiments to image the shapes of micron-sized crystals [5] and to measure the morphology of surfaces over many microns [6]. The latter example of a CXD reflectivity experiment benefits from the elongation of the beam footprint at small incidence angles, allowing a correspondingly longer region to be probed coherently. This happy situation is spoiled by the practical problems of transporting the beam from source to sample without distortion. In reality, a beamline needs optical components to handle heat load, vacuum, energy selection, etc. Unfortunately, these obligatory components can also affect the lateral coherence, sometimes seriously. This paper attempts to outline the origin of some of these problems and how they might be solved.

The simplest conceivable component is a beam aperture or slit. These are required for removing heat from the edges of the beam in order to protect other components. Slits are also needed to limit the divergence of the beam to restrict the illuminated area on a sample. In CXD experiments on nanocrystals, the number of illuminated crystals must be kept small enough that their individual diffraction patterns do not overlap [5]. In surface CXD reflectivity experiments, the imaged patch is defined entirely by crossed slits [6]. One of the practical limitations of designing a slit is that its edge is made of material with finite absorption, so will always be broadened slightly; a second problem is to provide a sufficiently well-defined, polished surface. Designs include finely polished Mo rollers [7] and even atomically flat cleaved surfaces of GaAs [8]. Even these suffer the fundamental limitation of Fresnel diffraction around the slit edge. So long as a macroscopic distance is needed between the slit and the sample, a broadened profile with a strong phase variation will certainly be introduced. A simple solution is to calculate the illumination function using classical optics [9]; this requires input knowledge of the surface properties of the slit material.

To appreciate the scale of the problem, consider the simple question of the resulting size of a beam cut from a plane wave by two slit blades separated by a distance x. To be useful, x should be in the range of a few microns. The slit needs to be placed a distance y, usually a few centimeters, in front of the sample. The shadow of the slit will have a width of x, but diffraction can increase the width considerably. For a rough estimate we can simply

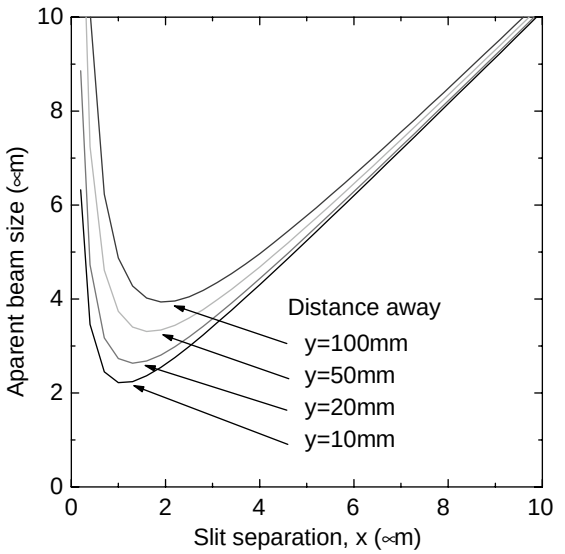

Fig. 1. Calculation of the beam size generated by a narrow slit of size x at distance y away. The broadening at small x is assumed to be due to Fraunhofer diffraction.

add the shadow width, x, to the Fraunhofer diffraction width of the central maximum, $\lambda y/x$. This result is plotted in Fig. 1 for $\lambda = 1.4$ Å and various values of y. The result is that there is a *minimum size* of the transmitted beam, which is at least a couple of microns even when the slit is as close as $y = 10$ mm. It is clearly not possible to make a beam smaller than this using slits.

One remedy is to incorporate the slit into the sample itself. This can be achieved by waveguide methods [10]. Another solution is to use focussing optics to make a small beam instead. Popular methods are compound refractive lenses, Fresnel zone plates and Kirkpatrick–Baez (KB) mirrors. As many authors have discussed, there are advantages and disadvantages of each of these methods [2]. Most of the discussion centers on achieving the smallest possible focus, but this is the situation that is worst for the destruction of the coherence. Optics can preserve the coherence even if they are not used to make the smallest focal spot: for example, a 10:1 demagnification leads to a theoretical 10 × improvement in flux at a cost of a 10 × reduction of the coherence length, which is acceptable in many situations. Imperfect optics will only worsen the performance.

As soon as transmitting or reflecting optics are introduced, we are left with a new source of decoherence, however. Any variations of thickness (transmission) or imperfections in the optical finish (reflection) will introduce phase variations in the resulting beam. In the case of a transmission object, it is the refractive index deviation (from unity) that couples the thickness variations to the resulting phase; in the case of reflection, it is the perpendicular momentum transfer (sine of the incidence angle) that couples the height variations to the phase. Windows, Be or otherwise, that are introduced to separate vacuum regions of the beamline will also act similarly as transmission objects. It is usually the phase, rather than amplitude, variations that cause problems, which are accentuated by the large distances between typical components [11]. We and others have developed a formalism that allows us to calculate the effects of partial coherence in diffraction experiments [12,13]. We have further attempted to model the imperfections of a typical optical element by an amplitude and lateral length scale, as in conventional theories of roughness [14]. Both amplitude and phase variations contribute, with the latter becoming more important with distance [15].

The results of this theory [15] can be understood as the generation of a "secondary source" at the location of the imperfect optical component, as Fig. 2 illustrates. A diverging swath of radiation intercepts the optic and interacts with it everywhere that is illuminated. Regardless of the detailed mechanism, whether it is absorption, scattering or refraction, a new component is generated that is incoherent with the original beam. This weak second component can be considered to be superposed on top of the original beam. Once this is accepted, most of the important properties can be calculated by simple geometry; it is only the magnitude of the effect that is hard to predict [15].

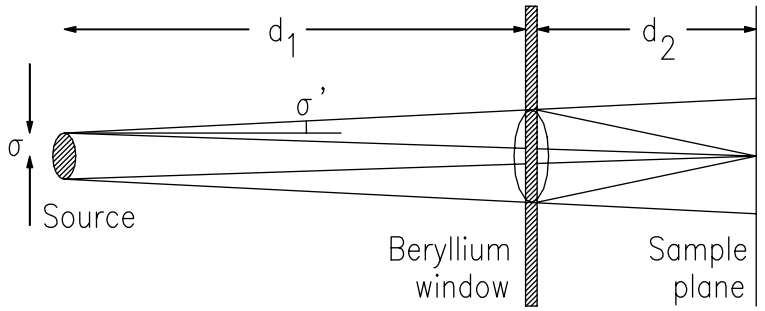

Fig. 2. Ray diagram showing how the coherence seen at the sample plane can acquire a secondary component due to the rescattering by a window. Symbols are those used in the text.

The first important conclusion is that the effect of optics is more serious than just an attenuation mechanism. Some of the beam is lost by outward scattering, but some of the beam is scattered inwards as well. Wherever the sample is sitting beyond the optical element, it receives a secondary component of illumination from the *entire* area of the optical element. This second component has considerably worse coherence than the original source: if nothing else is done to limit it, the source divergence σ' (angle) will determine the coherence length of the secondary component. Simple geometry in Fig. 2 then yields the following expression,

$$L_{T2} = \frac{\lambda D}{4\sigma} \frac{(1 - d_1/D)}{(1 + \alpha d_1/D)}, \quad (2)$$

where $\alpha = \sigma' D/\sigma$ is a dimensionless beam-expansion factor, the ratio of the diverged beam size at the sample to the original source size. The expression has been written in terms of the total source-sample distance, $D = d_1 + d_2$, for comparison with expression (1) for L_T due to just the source itself. Two multiplying factors appear in Eq. (2) that both contribute to a reduced coherence length. The numerator represents the effect of the closer optic-to-sample distance than the original source; this has a big effect when the optical element is close to the sample, which is a common situation. The denominator represents the divergence of the beam; the numerical factor α is about 3 in the horizontal and about 20 in the vertical for a typical undulator beamline at advanced photon source (APS). The denominator is also a big factor, since $\alpha \gg 1$.

We conclude that the window, or other optical element, acts as a secondary source that also contributes to the mutual intensity function (MIF). A beamline with such an element will generate a beam which is characterized by a *two-component* MIF, with one component coming from the X-ray source (undulator) and the second coming from the window. This picture is sketched in Fig. 3 assuming Gaussian distributions. The relative amplitude of the two components depends on the details of the imperfections of the optical element: roughness, impurities, density variation, etc. For a refractive optic, it depends as well on the distance away. The amplitude of the second component can be difficult to calculate [15], but the coherence length is very easy because it depends only on geometry. The relative widths of the two components in Fig. 3 are therefore given simply by expressions (1) and (2). Each contributing optical element in the beamline adds a component to the MIF, which will acquire a "wedding cake" appearance. Since the geometric factors in Eq. (2) can be large, this function can be very different from Gaussian, with long tails and a sharp center.

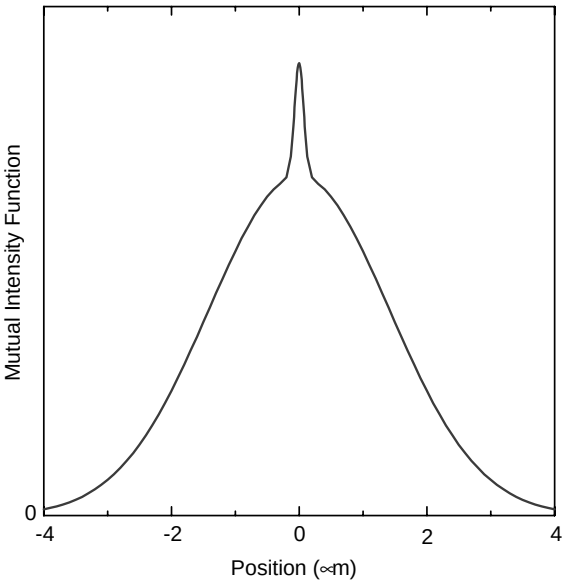

Fig. 3. Sketch of the mutual intensity function expected for an X- ray beam after passing through a Be window, as constructed in Fig. 2. The amplitude of the second (sharp) component is a strong function of the window's imperfections, but its width is given by geometry alone.

In CXD imaging experiments, we have already determined that the "hot spot" which appears near the center of reconstructed images can be associated with this unusual coherence function [12]. This was subsequently demonstrated in a more explicit calculation using typical beamline dimensions [15]. Noting that the standard way to measure coherence is to examine the contrast in a Young's double-slit experiment [9], we consider the CXD imaging experiments to be one way that the coherence propagation ideas discussed above can be tested, but this is rather indirect.

We now turn to our attempts to verify some of these ideas experimentally using the new 34-ID-C beamline at the APS. The beamline consists of an Undulator A [4], commissioning windows at 25 m, a horizontally deflecting mirror at 30 m [16], double-crystal monochromator at 47 m and exit window at 50 m. The sample would normally sit about 1 m beyond this last window and scatter into a detector on a long arm 3 m beyond. We developed a new high-resolution imaging detector for our tests. A commercial microscope with digital data acquisition and $200\times$ objective lens [17] was placed behind a cadmium tungstate single crystal. The direct, monochromatic beam gave a visible blue fluorescence signal that was sufficiently bright to fall within the autoranging sensitivity level of the microscope. Example images are shown in Fig. 4 of a $0.5\times0.5\ \mathrm{mm}^2$ beam with a spatial resolution of about 2 μm.

Fig. 4 shows an image of the 34-ID-C beam after passing through a Be foil. The foil was supplied commercially for use as a vacuum window in a beamline flight path, but was not of especially high quality. Transmission images are shown of different regions at three different distances, 350, 1300 and 2100 mm from foil to detector. The larger distances favor the phase-contrast mechanism, which appears as intensity variation in the transmitted images shown. Two characteristic features are seen: shadows and

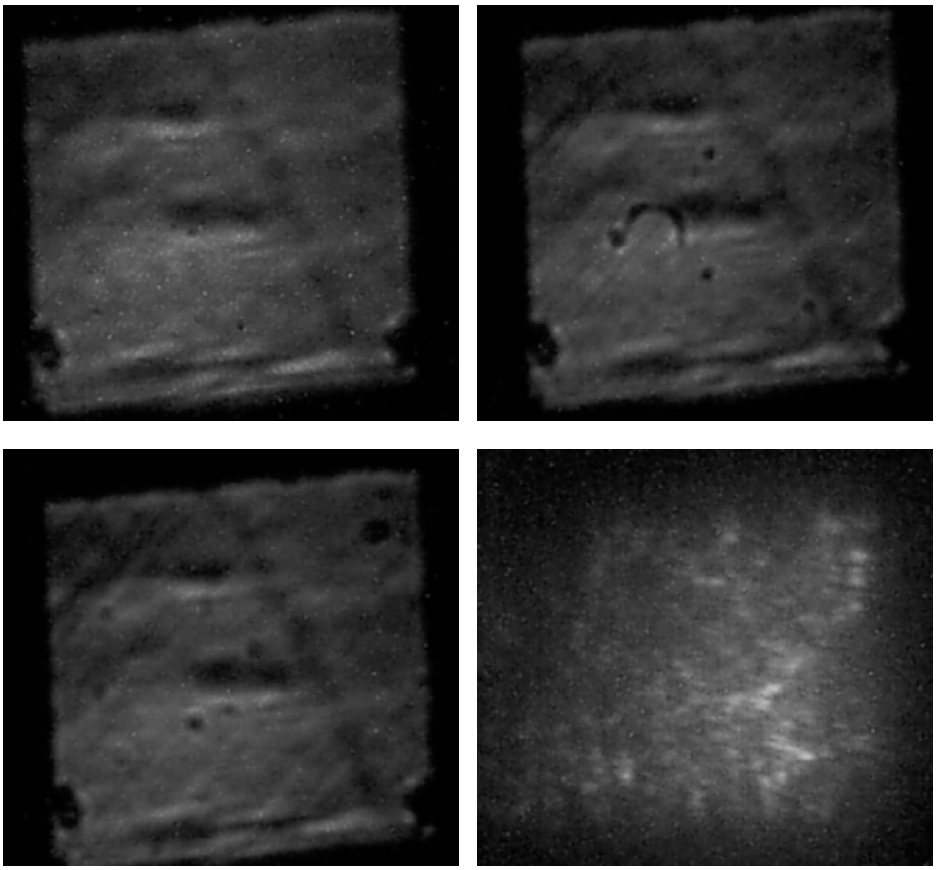

Fig. 4. High-magnification images of a 0.5×0.5 mm beam at beamline 34-ID-C of APS passing through a Be foil of rather poor quality. The detector was at a distance of 350 mm (top left), 1300 mm (top right) and 2100 mm (bottom left) behind the foil. The phase contrast mechanism causes the defects to be more visible at the larger distance. The bottom right image was taken through a BN window coating that was subsequently removed. The distance from the coating to the detector was 2400 mm.

scratches. The shadows are presumably due to heavy impurities that absorb the beam. They appear as dark circles about 2 μm in diameter in the 350 mm image and as larger fringed rings in the 1300 and 2100 mm images. The development of fringes is due to Fresnel diffraction around the inclusions. The diagonal scratches are surface features visible on the foil. They were placed at 45° to avoid confusion with the pixelation direction. They are barely discernable in the 350 mm image, become clearer in images at 600 mm (data not shown) and 1300 mm, before fading away in the 2100 mm image. Again, this identifies a phase contrast mechanism associated with refraction by the scratches. The apparent fading is due to the broadening of the features until they merge together.

Both of these features can be seen in the static images of Fig. 4, but they are much more dramatic when viewed as movies acquired while the foil is translated sideways across the beam (not shown). In movie format [17], it is very clear which features are moving against a static background of other contrast in the images. At the present time, it has not been possible to observe a featureless flat-field beam. The beamline components mentioned above contribute to a substantial background structure. Most prominent was the double-crystal monochromator which uses diamond (1 1 1) reflections. Here, topographic strain contrast was visible in the transmitted beam as angled ridges of intensity; these can be detected in the background of Fig. 4, visible as a non-moving features which are the same on all three images. Once again, the critical test was to translate the monochromator while recording a movie; all the ridges were found to move together. The movie technique is highly recommended as it gives immediate results about which optical element is the origin of each set of fine features in the beam. The intensity variation and the length scale of the contrast, seen far back from all optical components, are crude, but effective, measures of the extent to which the optics distorts the beam from an ideal plane wave.

Tests by moving other beamline components concluded that these did not contribute visibly to the contrast, as measured in this way. Small changes of the mirror angle were not detectable. It was not, however, possible to move the "commissioning window" which contains several fairly thick Be foils in its construction. Nevertheless, it was apparent from the tests in Fig. 4 that, for a given defect length scale, there was a *worst* distance for generating contrast in the beam image. Very close to the foil, the phase contrast has not yet developed, while very far away the contrast features have broadened sufficiently so as to become diffused away. For typical materials, this worst distance seems to be a few meters. This may explain why the mirror and commissioning window did not appear to cause trouble. We note that this conclusion is based on data measured by a camera with 2 μm resolution; if a finer (or coarser) scale was accessible, our conclusion might be different. Fig. 4 does suggest, however, that the micron length scale is the relevant one for defects of Be, and may explain why Be was suspected early on as an experimental difficulty in CXD experiments [18]. The variation of phase contrast with distance in Be confirms the earlier findings at other third-generation sources, such as ESRF [11].

Finally, we show in Fig. 5 a dramatic example of the effect of coherence on the bottom line: the resulting CXD diffraction patterns from a 0.5 μm nanocrystal of Au. The objective of these experiments is to study the external surfaces of these model nanocrystals to see how this affects the physical properties of the nanophase [5]. The left image in Fig. 5 was taken in the initial configuration of the 34-ID-C beamline in March 2002. A temporary Be window was installed at the end of the beamline at 50 m, about 1 m in front of the sample. To protect the window from corrosion in the pink-beam mode of operation, the window had been coated with a thin film of BN dry lubricant. While the transmission of the window appeared satisfactory, the high resolution spatial images of the beam taken through this BN coating were very bad, as the last image in Fig. 4 shows. The wavefront has become broken up into blotches and the $0.5 \times 0.5\ \mathrm{mm}^2$ slit borders have become indistinct. After installation of the final beamline window in October 2002, the CXD image from the same sample (not the same nanocrystal) shows respectable contrast on the right side of Fig. 5.

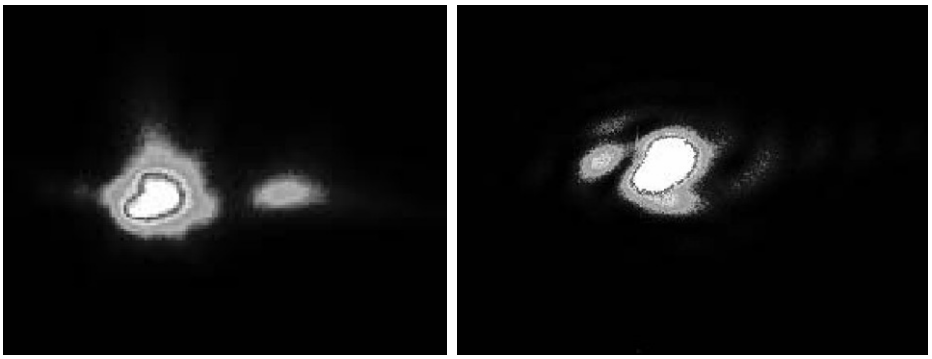

Fig. 5. Measured CXD diffraction patterns of the (1 1 $\bar{1}$) reflection of 0.5 μm Au nanocrystals under different beam conditions. A CCD detector with 22.5 μm pixels was located 2.8 m from the sample, giving a resolution of 3.7×10^{-5} Å^{-1} per pixel. Left: with a BN spray coating on the exit window located 0.8 m before the sample. Right: with the coating removed. Note that the patterns do not come from the same grain in the sample.

The 34-ID-C CXD facility was constructed with the help of a Major Research Instrumentation grant DMR 97-24294 from the NSF. The UNICAT facility at the Advanced Photon Source (APS) is supported by the University of Illinois at Urbana-Champaign, Materials Research Laboratory (DOE DEFG02-91ER45439, the State of Illinois-IBHE-HECA, and the NSF), the Oak Ridge National Laboratory (US DOE under contract with UT-Battelle LLC), the National Institute of Standards and Technology (US Department of Commerce) and UOP LLC. The APS is supported by the US DOE, Basic Energy Sciences, Office of Science under contract No. W-31-109-ENG-38.

References

[1] M. Sutton, S.G.J. Mochrie, T. Greytak, S.E. Nagler, L.E. Berman, G.A. Held, G.B. Stephenson, Nature 352 (1991) 608.
[2] B. Lengeler, Naturwissenschaften 88 (2001) 249.
[3] J. Als-Nielsen, D. McMorrow, Elements of Modern X-ray Physics, Wiley, New York, 2001.
[4] R.J. Dejus, B. Lai, E.R. Moog, E. Gluskin, Argonne National Laboratory report ANL/APS/TB-17, 1994.
[5] I.K. Robinson, I.A. Vartanyants, G.J. Williams, M.A. Pfeifer, J.A. Pitney, Phys. Rev. Lett. 87 (2001) 195505.
[6] I.K. Robinson, J.L. Libbert, I.A. Vartanyants, J.A. Pitney, D.M. Smilgies, D.L. Abernathy, G. Grübel, Phys. Rev. B 60 (1999) 9965.
[7] J.L. Libbert, J.A. Pitney, I.K. Robinson, J. Synchrotron Radiat. 4 (1997) 125.
[8] Y. Yacoby, R. Pindak, R. MacHarrie, L. Pfeiffer, L. Berman, R. Clarke, J. Phys.: Condens. Matter 12 (2000) 3929.
[9] M. Born, E. Wolf, Principles of Optics, Pergamon Press, London, 1970.
[10] F. Pfeiffer, C. David, M. Burghammer, C. Riekel, T. Salditt, Science 297 (2002) 230.
[11] A. Snigirev, I. Snigireva, V. Kohn, S.M. Kuzretsov, Nucl. Inst. Meth. A 370 (1996) 634.
[12] I.A. Vartanyants, I.K. Robinson, J. Phys.: Condens. Matter 13 (2001) 611.
[13] M. Tolan, S.K. Sinha, Phys. B 248 (1998) 399.
[14] S.K. Sinha, E.B. Sirota, S. Garoff, H.B. Stanley, Phys. Rev. B 38 (1988) 2297.
[15] I.A. Vartanyants, I.K. Robinson, Phys. Rev. B (2002), submitted for publication.
[16] C.A. Benson, I.K. Robinson, Beam splitting mirror for advanced photon source sector 34, in: P. Pianetta, et al. (Eds.), AIP Conference Series: 11th US National Conference on Synchrotron Radiation Instrumentation, Vol. CP521, 2000, pp. 230–233.
[17] "Intel-Play", QX3 Computer Microscope. Intel Corp. 2001.
[18] E. Dufresne, Ph.D. Dissertation, McGill University, 1995.